Liu Yu (Orcid ID: 0000-0002-1402-0737)

Cai Wenju (Orcid ID: 0000-0001-6520-0829)

Li Jianping (Orcid ID: 0000-0003-0625-1575)

Leavitt Steven (Orcid ID: 0000-0002-7291-208X)

Ng Benjamin (Orcid ID: 0000-0002-4458-4592)

Cherubini Paolo (Orcid ID: 0000-0002-9809-250X)

Wang Guojian (Orcid ID: 0000-0002-8881-7394)

Chen Deliang (Orcid ID: 0000-0003-0288-5618)

Linderholm Hans, Wilhelm (Orcid ID: 0000-0002-1522-8919)

Anthropogenic aerosols cause recent pronounced weakening of Asian Summer Monsoon relative to last four centuries

Yu Liu[1*, 2, 3, 4], Wenju Cai[3, 5, 6, 1], Changfeng Sun[1], Huiming Song[1, 3], Kim M. Cobb[7], Jianping Li[3, 5], Steven W. Leavitt[8], LixinWu[3], Qiufang Cai[1, 3], Ruoshi Liu[9], Benjamin Ng[6], Paolo Cherubini[10], Ulf Büentgen[11, 10, 12], Yi Song[1], Guojian Wang[3, 6], Ying Lei[1], Libin Yan[1], Qiang Li[1, 3], Yongyong Ma[13], Congxi Fang[1], Junyan Sun[1], Xuxiang Li[9], Deliang Chen[14], Hans W. Linderholm[14]

This article has been accepted for publication and undergone full peer review but has not been through the copyediting, typesetting, pagination and proofreading process which may lead to differences between this version and the Version of Record. Please cite this article as doi: 10.1029/2019GL082497

[1] The State Key Laboratory of Loess and Quaternary Geology, Institute of Earth Environment, Chinese Academy of Sciences, Xi'an 710061, China.

[2] CAS Center for Excellence in Quaternary Science and Global Change, Chinese Academy of Sciences, Xi'an 710061, China.

[3] Laboratory for Ocean Dynamics and Climate, Pilot Qingdao National Laboratory for Marine Science and Technology, Qingdao, 266237, China.

[4] Interdisciplinary Research Center of Earth Science Frontier (IRCESF) and Joint Center for Global Change Studies (JCGCS), Beijing Normal University, Beijing 100875, China.

[5] Physical Oceanography Laboratory/CIMST, Ocean University of China and Qingdao National Laboratory for Marine Science and Technology, Qingdao 266100, China.

[6] CSIRO Marine and Atmospheric Research, Aspendale, Victoria, Australia.

[7] School of Earth and Atmospheric Sciences, Georgia Institute of Technology, Atlanta, Georgia 30332, USA.

[8] The Laboratory of Tree-Ring Research, The University of Arizona, Tucson, Arizona 85721, USA.

[9] School of Human Settlements and Civil Engineering, Xi'an Jiaotong University, Xi'an 710049, China.

[10] Swiss Federal Institute for Forest, Snow and Landscape Research, Zürcherstrasse 111, CH-8903 Birmensdorf, Switzerland

[11] Department of Geography, University of Cambridge, CB2 3EN, UK.

[12] Global Change Research Centre and Masaryk University, 613 00 Brno, Czech Republic.

[13] Shaanxi Meteorological Observatory, Xi'an, 710014, China.

[14] Regional Climate Group, Department of Earth Sciences,University of Gothenburg, S-405 30 Gothenburg, Sweden

*Corresponding author:

The State Key Laboratory of Loess and Quaternary Geology, Institute of Earth Environment, Chinese Academy of Sciences

Address: No. 97 Yanxiang Road, Xi'an 710061, Shaanxi, China

Phone: 86-29-62336225; Cell phone: 86-13359291673; Fax: 86-29-62336234;

Email: liuyu@loess.llqg.ac.cn

Key Points

A 448-year Asian Summer Monsoon reconstruction that extends back to 1566 AD was developed using an ensemble of ten tree-ring chronologies from northwest China.

The recent 80-year decreasing trend of the Asian Summer Monsoon was unprecedented over the past 448 years.

Coupled climate models showed that the unprecedented decreasing trend was likely due to increasing anthropogenic aerosols.

Abstract

The Asian Summer Monsoon (ASM) affects ecosystems, biodiversity, and food security of billions of people. In recent decades, ASM strength (as represented by precipitation) has been decreasing, but instrumental measurements span only a short period of time. The initiation and the dynamics of the recent trend are unclear. Here for the first time, we use an ensemble of ten tree-ring width chronologies from the west-central margin of ASM to reconstruct detail of ASM variability back to AD 1566. The reconstruction captures weak/strong ASM events and also reflects major locust plagues. Notably, we found an unprecedented 80-year trend of decreasing ASM strength within the context of the 448-year reconstruction, which is contrary to what is expected from greenhouse warming. Our coupled climate model shows that increasing anthropogenic sulfate aerosol emissions over the Northern Hemisphere could be the dominant factor contributing to the ASM decrease.

Plain Language Summary

Monsoonal rainfall has a certain influence on agriculture and industry in the regions of Asian Summer Monsoon (ASM). An understanding of the spatial-temporal variability of the ASM and the associated dynamics is vital for terrestrial ecosystems, water resources, forests, and landscapes. We have developed a 448-year ASM reconstruction back to 1566 AD using ten tree-ring chronologies from the margin region of ASM. We find that historical severe droughts and locust plague disasters during weak ASM events. The recent decreasing ASM trend persisting for over 80 years is unprecedented over the past 448 years. Coupled climate models show that increasing anthropogenic aerosol emissions are the dominant underlying factor. Our aim is that the time series will find a wide range of utility for understanding past

climate variability and for predicting future climate change.

Keywords: Asian Summer Monsoon; tree-ring chronology; precipitation reconstruction; anthropogenic aerosol

1. Introduction

The Asian Summer Monsoon (ASM) results from a sea-land thermal contrast driven by solar radiation that varies by seasons. The monsoonal precipitation is closely related to agriculture and industry in most of China, especially in the margin region of the ASM. This region is located parallel to the 200–400 mm rainfall isohyets in China (Figures 1a and 1b) (Liu et al., 2014), and is a transition zone between arid and semiarid conditions and between deserts and the loess belt. Approximately 70%–90% of the regional annual precipitation occurs in boreal summer and is strongly influenced by ASM (Wang, 2006). An understanding of the spatial-temporal variability of the ASM and the associated dynamics is vital for management of terrestrial ecosystems, water resources, forests, and landscapes (Liu et al., 2017; Piao et al., 2010; Wang, 2006). Several forcing factors may affect the strength of the ASM, including solar variability, volcanic eruptions and anthropogenic aerosols. Anthropogenic aerosol forcing (Bollasina et al., 2011; Cai et al., 2017; Ganguly et al., 2012; Kim et al., 2016; Lau & Kim, 2006; Song et al., 2014; Zhu et al., 2012) is of particular interest given that concentration of aerosols in China, especially in northwest China, has been increasing over the past several decades. However, how aerosols and the ASM interact is not fully understood yet (Li et al., 2016; Wu et al., 2016).

Understanding past variability of the ASM is important for detection and attribution of its recent and future changes. Observational studies of the modern ASM system in terms of its sub-components, onset time, seasonal cycle, moisture sources, external forcing and its dynamic changes (Ding & Chan, 2005; Li et al., 2015; Ueda et al., 2015; Waliser et al., 2003), have revealed a three-decade trend of decreasing ASM since the end of the 1970s (Wang, 2001). Putting this trend in a long-term context is essential in order to identify whether it is caused by natural variability or anthropogenic forcing, and to examine the associated dynamics. To this end, the properties of the recent ASM decreasing trend, including whether it is a part of a longer-term trend must be understood, but available instrumental measurements cover only a short period of time.

In this study, we construct a 448-year ASM time series back to AD 1566 using an ensemble of ten tree-ring width chronologies from the western Loess Plateau, China. The relationship between the recent 80-year decreasing ASM trend, which was unprecedented over the past four centuries, and the increasing anthropogenic aerosol is also examined.

2. Materials and Methods

2.1. Tree-ring chronologies and meteorological data

Ten tree-ring chronologies, including 584 cores from 310 trees, over the ASM fringe were employed in this study (Figure 1a, Table S1). Chronologies from Mt. Shoulu, Mt. Shouyang, Zunisi and Tulugou (two chronologies at the site) were previously published data (Liu et al., 2013a, 2013b; Song et al., 2017; Sun et al., 2018). Chronologies from Mt. Helan, Mt. Kongtong, Mt. Xinglong and Mt. Hasi were update data and the old chronologies from these sites were published (Liu et al., 2005, 2013c; Ma et al., 2015; Song & Liu 2011). The

chronology from Mt. Guiqing has not been published yet. Cores from a minimum of 20 individual trees were collected using increment borers at each site. Each chorology has a strong local precipitation signal (Fang et al., 2010; Liu et al., 2005, 2013a, 2013b, 2013c; Ma et al., 2015; Song & Liu 2011; Song et al., 2017; Sun et al., 2018), and the correlation coefficients among them are statistically significant (Table S2). LINTAB system was used to measure tree-ring widths of each core with an accuracy up to 0.001mm. Cross-dating was applied to assign each tree ring to the calendar year of its formation, it is based on the recognition that trees exhibit similar year-to-year growth changes when growing in the same period and under the same climate condition (Fritts, 1976).

We assembled all individual cores from each of the ten sites to generate a single ring-width chronology that covers the ASM fringe region using ARSTAN (Cook & Kairiukstis, 1990). Straight line or a negative exponential function was used to fit growth trend of the trees due to non-climatic effects. Specifically speaking, a dimensionless index for each tree-ring core was computed by dividing each ring's original measurement by the fitted curve's value in the corresponding year. And by running a bi-weight robust mean method, the stable variance technique was additionally employed in building the chronology. Three types of chronologies were generated by the ARSTAN program: standard, residual and autoregressive chronologies. We chose the standard (STD) chronology for analysis, since it contains both high- and low-frequency signals. EPS (Expressed Population Signal) during AD 1566–2013 in our chronology reached 0.85, an acceptable threshold for a reliable chronology (Wigley et al., 1984). A minimum of 9 cores contributed to the chronology in AD 1566 (Figure S1, Table S3).

The observed precipitation and temperature data (1951–2013) from 39 meteorological stations at the ASM northwestern margin were used (Figure 1a, Table S4). To study the climate response of tree growth in the ASM fringe region, the means of the meteorological data was to taken as the regional climatic condition. The regional monthly precipitation and temperature are given in Figure S2a.

2.2. Transfer function and its calibration and verification

Correlation function analyses showed that over the 1952–2013 period, the STD chronology had significantly positive correlations with the regional precipitation from previous-year July to current-year June (P_{JJ}, Figure S2b). As such, the regional tree-ring chronology effectively tracks precipitation at the margin. Thus, applying the simple linear regression model, a transfer function was designed: P_{JJ}=140.644*Wt + 198.455 (r=0.766, R^2=0.586, R^2_{adj}=0.579, N=62, p<0.0001), where "Wt" means the regional tree-ring standard chronology at year t.

About 58.6% of the observed variance could be explained by the reconstruction over the calibration periods from 1952 to 2013. Figure 1c illustrates that the reconstruction tracked the observed precipitation closely. A split-sample method was used to verify the reliability and stability of the regression equation (Cook et al., 1999; Fritts, 1991). To perform validation, we calibrated climate data from one sub-period (both 1983-2013 and 1952-1982) and verified the reconstruction with the remaining data (1952-1982 and 1983-2013, respectively). To perform verification, correlation coefficient (r), explained variances (R^2), sign test (ST), reduction of error (RE), coefficient of efficiency (CE) and the product means test (t) were used. Rigorous model skill was indicated by values of RE and CE greater than zero (Cook et al., 1999). All these statistical parameters suggested that our regression model was highly

stable and reliable (Table S5), especially *RE* and *CE*, indicating that the reconstructed P_{JJ} time series can be regarded as a proxy of precipitation over the ASM fringe region. Because the relationship between the tree-ring chronology and reconstructed P_{JJ} series is linear, they could represent each other. We therefore used the reconstructed P_{JJ} series in the subsequent analyses.

3. Results

3.1. Moisture source of the ASM and utility of the reconstruction

Precipitation over the ASM northern margin originates from moisture transport by the South Asian Monsoon and East Asian Monsoon (Ding & Chan, 2005). Below 700 hPa (elevation 3000 m and lower), like other regions of ASM, such as the lower reaches of the Yangtze River, the water vapor in July–September originates from the Indian Ocean and the western Pacific (Figure 2a). However, due to the Rossby wave response, Pacific-Japan pattern, across the East Asia, an anomalous anticyclone exists over the western North Pacific and an anomalous cyclone always accompanies the anomalous anticyclone at its north during weak ASM periods (Feng et al., 2014). There are northerly anomalies at the west of the anomalous cyclone. Such circulation anomalies make the northward water vapor transport decrease in the north of China but increase the water vapor convergence in the lower reaches of the Yangtze River (Wang et al., 2008). Once the ASM weakens, the north may experience drought as the water vapor supplement is deficient, but it may not be always humid everywhere in the south, because the convergence anomaly distributes like a belt which may be located at different latitudes under various atmospheric circulation anomalies (Wang et al., 2001; Feng et al., 2014). Therefore, the precipitation at the northern margin is more sensitive

to the strengthening/weakening of the ASM (Ding et al., 2008; Wang et al., 2008) and can be regarded as a proxy for the ASM. Indeed, the observations over the period 1951–2013 from the 39 stations within the fringe region show that precipitation of July–September of previous year accounts for 56.7% of the precipitation from July of previous year to June of current year, i.e., P_{JJ}. In addition, the observed P_{JJ} had a significant correlation with July–September precipitation of most regions in the north of China (Figure S3a). Furthermore, over the same period, the reconstructed P_{JJ} has the strongest correlation with observed precipitation in July, August, and September of the previous year, i.e., the peak season of the ASM (Figure 2b). The correlation between the reconstructed P_{JJ} series and July−September precipitation of the previous year reached 0.574. In addition, the reconstructed P_{JJ} series has significant correlation with the previous-year July−September precipitationreconstructed for the ASM fringe, differences from other ASM indices (Li & Zeng, 2002; Wang & Fan, 1995) are expected, as those other indices focus on east Asia/China or south Asia/China. Several tree-ring based ASM reconstructions exist, but most only used one or two tree-ring sites from the Tibetan Plateau (Grießinger et al., 2011; Li et al., 2008; Xu et al., 2012). There was a monsoon index reconstructed using multiple sites from the monsoon region, but it primarily focuses on the South Asian monsoon change (Shi et al., 2014, 2017). Ten tree-ring chronologies used in this study are highly responsive to monsoon precipitation in the fringe regions of ASM, and thus our reconstructed series are more sensitive to monsoon changes and show some distinct differences from other ASM reconstructions (Figure S4).

3.2. Validation by historical events and known knowledge

The ASM surrogate of P_{JJ} reproduces known historical extreme events described in historical documents (Compilation of China meteorological disaster Canon, 2006; Yuan, 1994), and documented in a dryness/wetness index (DWI) over China (Chinese Academy of Meteorological Sciences, 1981; Zhang et al., 2003), which was constructed using historical documents with climatic descriptions, such as local annals. A reduced P_{JJ} is seen when the DWI is high (Figure 3a). Historical documents of the ASM northern margin recorded several large-scale severe drought events including 1586/87, 1759, and 1928/29, particularly in Shaanxi, Gansu and Ningxia (Compilation of China meteorological disaster Canon, 2006; Yuan, 1994) (stippled area in Figure 1b), which were postulated to be the result of dramatic weakening of the ASM. During 1586/87, more than half the population in eastern Gansu fled their homeland, and there was a report of cannibalism. In 1759, food prices skyrocketed and severe famine plagued the region of Gansu (Yuan, 1994). In 1928 and 1929, a severe drought hit north China, including the three provinces; more than 500,000 people lost their lives because of famine and there were reports of dogs eating human bodies and family suicide (Compilation of China meteorological disaster Canon, 2006; Ge et al., 2016; Yuan, 1994). These drought events were all captured in the P_{JJ} time series (Table S6), which supports a weakened ASM causing these droughts.

That the P_{JJ} time series is an appropriate surrogate for the ASM is further corroborated by locust plagues at the ASM margin during the historical period (Li 2008; Tian et al., 2011), in which valuable crops were devoured by plagues of locusts, exacerbating the impact of

droughts on crop yields and leading to severe starvation. Such plagues are seen to coincide with the dry years in the P_{JJ} time series (Figure 3b), especially during periods of extreme droughts (Table S7).

The P_{JJ} also reproduces marked variations (Figures 3 and S5) that are found in other paleoclimate series from different proxies (Qian et al., 2011; Zhang et al., 2008). These include the dominant 24-year cycles (Figures 3c and S6), which coincide with a 23-year cycle found in a thousand-year-long DWI in East Asia using six summer dry-wet modes in eastern China (Qian et al., 2011), and 2.5–2.8-year cycles, which reflect a typical feature of Asian monsoon variations (Wu & Kirtman, 2004). The index series in Qian et al. (2011) is longer, but it is a qualitative description of the East ASM with only six different modes. Our series, on the other hand, is a quantitative representative for ASM.

3.3. Recent ASM weakening and the effect of anthropogenic aerosols

The utility of our reconstruction transcends direct examination, confirmation and reproduction of historical events, as it extends to the debate about recent climate change, particularly how the ASM may respond to climate change. Available rainfall observations show that there is a decline in the ASM (i.e., three to four decades) (Xu et al., 2006; Zhu et al., 2012), but the observations cover a relatively short period. The P_{JJ} time series also showed that there was a decline in recent decades. To find out the significant and longest decreasing trend of the ASM, we calculated the 50-year, 55-year, 60-year, 65-year, 70-year, 75-year, 80-year, 85-year and 90-year running trend for the reconstructed P_{JJ} during 1566–2013 (Figure S7). The longest and significant declining trend in recent decades occurred in the 80-year running trend analysis. In addition, the remarkable 80-year decreasing trend during

the period 1934–2013 (Figure 4a) is the largest in the entire 448 years under the 80-year sliding windows (Figure 4b). This 80-year decreasing trend is similar with the significant weakening of precipitation during the recent 100 years in the Indian monsoon region (Xu et al., 2016). It is likely because that precipitation in this study represent the changes of both Indian monsoon and East Asian monsoon, therefore, the P_{JJ} series shows a decreasing trend in recent 100 years with value of ca. 0.14mm/y, but it does not exceed the 95% significant level.

Due to the different external forcings, the outcome of the projection from a radiative forcing scenario dominated by greenhouse warming, under which land would warm faster than ocean and the land-sea thermal contrast would increase (Christensen et al., 2013), indicated the ASM was enhanced in recent decades, which differs from our result. Therefore, there are likely other forcings leading to the weakening ASM. In the search for a dynamical cause, we found that neither the Pacific Decadal Oscillation (Watanabe & Yamazaki, 2014) nor the North Atlantic Oscillation (Lu et al, 2006) can account for this 80-year decreasing trend (Figure S8).

A forcing scenario in which increasing anthropogenic aerosols dominate was then considered (Bollasina et al., 2011). Although emissions of the black carbon over western Asia enhance pre-monsoonal rainfall over the Indian subcontinent but suppress pre-monsoonal rainfall across East Asia (Lau et al., 2006), sulfate emissions have been shown to force a reduction in ASM intensity (Lau et al., 2006; Menon et al., 2002). We postulate that this 80-year decreasing trend of the ASM in our P_{JJ} is a result of a sulfate aerosol-induced ASM reduction overwhelming an increasing greenhouse gas-induced enhancement.

We test our hypothesis by examining two sets of fully coupled climate experiments, each with eight ensemble members for 1871–1999 with the CSIRO coupled climate model (Rotstayn et al., 2007). The first set includes a time-varying radiative forcing from global emissions of solar irradiance, greenhouse gases, ozone, volcanic aerosols, and anthropogenic aerosols. The second set is the same as the first set except all anthropogenic aerosols are kept constant at the pre-industrial level. Both the direct and indirect effects of aerosols are parametrized and included. As Rotstayn et al. (2007) indicated that 'the model incorporated a comprehensive and interactive aerosol scheme and contained emissions of sulfate and carbonaceous aerosols, mineral dust, sea salt and stratospheric aerosols from volcanos.' Global emissions underwent a strong increase after about 1940 following World War II, but after 1980 sulfur emissions were reduced everywhere except Asia, where emissions have continued to increase to present (Smith et al., 2006).

Comparison of the ensemble mean of the two sets of experiments shows that the summer rainfall since 1940 in most regions of China, including the ASM margin, would increase without radiative forcing of anthropogenic aerosols (Figure 5a). However, when aerosol forcing is added, the ASM, including the ASM fringe region, decreases (Figure 5b). This impact from anthropogenic aerosols is clearly shown in time series of 21-year running averages over northern China encompassing the fringe region. There was low precipitation from 1920–1940 not associated with the radiatively-forced precipitation change (Figure 5c), which likely resulted from a positive PDO (Figure S8). However, the timing for the onset of the decreasing trend commenced around 1940 in this model (Figure 5c), approximately corresponding to that in the P_{JJ} time series. Thus, emissions of anthropogenic aerosols over a

hemispheric scale have the potential to drive the strongest ASM decreasing trend in the past 80 years, which is the strongest seen in our reconstructed ASM time series.

4. Conclusions and Discussion

Here a 448-year reconstruction targets the ASM by using ten tree-ring chronologies in the ASM fringe region, selected on the basis that they are sensitive only to rainfall, providing not only a higher-resolution, but also an appropriate and direct proxy of the ASM over reconstruction from previous studies. Our reconstruction provides an important time series to study the ASM over the past 448 years. The time-series confirms known properties of the ASM (Qian et al., 2011) (e.g., the 24-year frequency spectrum), reproduces known historical extreme climate events (Ge et al., 2016), and offers opportunities to understand less-known events (Tian et al., 2011).

Further, the reconstruction can contribute to the debate regarding the recent behavior of the ASM (Zhu et al., 2012), and help evaluate the relative importance of anthropogenic radiative forcing factors (Song et al., 2014). We find a decreasing trend of the ASM in the past 80 years, which is strongest decline of the past 448 years, but contrary to the expected increasing trend if influenced primarily by a greenhouse warming. Comparison of two sets of historical model experiments (10 run each) with and without increasing anthropogenic aerosols shows that this unprecedented decreasing trend is likely due to increasing anthropogenic aerosols, highlighting that the ASM-weakening effect of increasing anthropogenic sulfate aerosols could more than offset the ASM-enhancing effect of increasing greenhouse gases. Modelling is the only way to identify likely causes of the decreasing trend, and the results support a

mechanism that would otherwise be difficult to measure directly. Song et al. (2014) first quantitatively compared the anthropogenic aerosols among all other external forcings in the weakening of ASM during 1958–2001. This work further confirmed that anthropogenic aerosol's role in the ASM weakening in a longer period of 1934–2013. Of course, the increase of sulfate aerosols is the primary factor for the recent 80-year trend of weakening monsoon, and other factors, such as PDO and NAO, might have influences on the monsoon weakening, especially during historical periods without anthropogenic aerosols.

In summary, we expect that the time-series of the ASM at its northern margin will find a wide utility for understanding past climate variability in this region, and for detection and attribution for current climate change, beyond the examples that we provide.

Acknowledgments

This study was jointly supported by grants from the National Natural Science Foundation of China (41630531), the DQGG0104，Chinese Academy of Sciences (QYZDJ–SSW–DQC021, XDPB05 and GJHZ1777), the Institute of Earth Environment, Chinese Academy of Sciences and the State Key Laboratory of Loess and Quaternary Geology. Data are available via the NOAA online server.

References:

Bollasina, M. A., Ming, Y. & Ramaswamy, V. (2011). Anthropogenic Aerosols and the weakening of the South Asian summer monsoon. *Science* 334, 502–505.

Cai, W. J., Li, K., Liao, H., Wang, H. J. & Wu, L. X. (2017). Weather conditions conducive to Beijing severe haze more frequent under climate change. *Nature Climate Change*, 7, 257–262.

Chinese Academy of Meteorological Sciences, 1981. Yearly Charts of Dryness/Wetness in China for the Last 500-year Period. Beijing: SinoMaps Press, 322p

Christensen, J. H., Krishna Kumar, K., Aldrian, E., An, S.-I., Cavalcanti, I. F. A., de Castro, M., et al. (2013). Climate phenomena and their relevance for future regional climate change. In: Climate Change 2013: The physical science basis. Contribution of working group I to the fifth assessment report of the intergovernmental panel on climate change [Stocker, T. F. *et al.*, (Eds.)]. Cambridge University Press, Cambridge, United Kingdom and New York, NY, USA.

Compilation of China meteorological disaster Canon. (2006). China meteorological disaster Canon. China Meteorological Press, Beijing.

Cook, E. R. & Kairiukstis, L. A. (1990). Methods of Dendrochronology: Applications in the Environmental Sciences. *Kluwer Academic Publishers, Dordrecht*.

Cook, E. R., Meko, D. M., Stahle, D. W. & Cleaveland, M. K. (1999). Drought reconstructions for the continental United States. *Journal of Climate*, 12, 1145–1162.

Ding, Y. H. & Chan, J. C. L. (2005). The East Asian summer monsoon: an overview. *Meteorology and Atmospheric Physics*, 89, 117–142.

Ding, Y. H., Wang, Z. Y. & Sun, Y. (2008). Inter-decadal variation of the summer precipitation in East China and its association with decreasing Asian summer monsoon. Part I: Observed evidences. *International Journal of Climatology*, 28, 1139–1161.

Fang, K. Y., Gou, X. H., Chen, F. H., D'Arrigo, R. & Li, J. B. (2010). Tree-ring based drought reconstruction for the Guiqing Mountain: linkages to the Indian and Pacific Oceans. *International Journal of Climatology*, 30, 1137–1145.

Feng, J., Wang. L. & Chen, W. (2014). How Does the East Asian Summer Monsoon Behave in the Decaying Phase of El Nino during Different PDO Phases? *Journal of Climate*, 27(7), 2682–2698.

Fritts, H. C. (1976). Tree rings and climate. *Academic Press, London*.

Fritts, H. C. (1991). Reconstructing large-scale climatic patterns from tree-ring data. *The University of Arizona Press, Tucson*.

Ganguly, D., Rasch, P. J., Wang, H. L. & Yoon, J. H. (2012). Climate response of the South Asian monsoon system to anthropogenic aerosols. *Journal of Geophysical Research Atmospheres*, 117, D13209.

Ge, Q. S., Zheng, J. Y., Hao, Z. X., Liu, Y. & Li, M. Q. (2016). Recent advances on reconstruction of climate and extreme events in China for the past 2000 years. *Journal of Geographical Sciences*, 26, 827–854.

Grießinger, J., Bräuning, A., Helle, G., Thomas, A. & Schleser, G. (2011). Late Holocene Asian summer monsoon variability reflected by $\delta^{18}O$ in tree-rings from Tibetan junipers. *Geophysical Research Letters*, 38, L03701.

Kim, M. J., Yeh, S. W., & Park, R. J. (2016). Effects of sulfate aerosol forcing on East Asian

summer monsoon for 1985–2010. *Geophysical Research Letters*, 43, 1364–1372.

Lau, K. M. & Kim. K. M. (2006). Observational relationships between aerosol and Asian monsoon rainfall, and circulation. *Geophysical Research Letters*, 33, L21810.

Lau, K. M., Kim, M. K. & Kim, K. M. (2006). Asian summer monsoon anomalies induced by aerosol direct forcing: the role of the Tibetan Plateau. *Climate Dynamics*, 26, 855–864.

Li G. (2008). An integrated study on record characteristics and environmental significance of locust plagues in China during the historical period. Doctoral thesis, Lanzhou University, Lan Zhou.

Li, J. B., Cook, E. R., D'Arrigo, R., Chen, F. H., Gou, X. H., Peng, J. F., et al. (2010). Common tree growth anomalies over the northeastern Tibetan Plateau during the last six centuries: implications for regional moisture change. *Global Change Biology*, 14, 2096–2107.

Li, J. P. & Zeng, Q. C. (2002). A unified monsoon index. *Geophysical Research Letters*, 29, 1274.

Li, X. Q., Ting, M. F., Li, C. H. & Henderson, N. (2015). Mechanisms of Asian Summer Monsoon Changes in Response to Anthropogenic Forcing in CMIP5 Models. *Journal of Climate*, 28, 4107–4125.

Li, Z. Q., Lau, W. K. M., Ramanathan, V., Wu, G., Ding, Y., Manoj, M. J., et al. (2016). Aerosol and monsoon climate interactions over Asia. *Reviews of Geophysics*, 54, 866–929.

Liu, J. B., Rühland, K. M., Chen, J. H., Xu, Y. Y., Chen, S. Q., Chen, Q. M., et al. (2017). Aerosol-weakened summer monsoons decrease lake fertilization on the Chinese Loess

Plateau. *Nature Climate. Change*, 7, 190–194.

Liu, Y., Cai, Q. F., Shi, J. F., Hughes, M. K., Kutzbach, J. E., Liu, Z. Y., et al. (2005). Seasonal precipitation in the south-central Helan Mountain region, China, reconstructed from tree-ring width for the past 224 years. *Canadian Journal of Forest Research*, 35, 2403–2412.

Liu, Y., Lei, Y., Sun, B., Song, H. M. & Li, Q. (2013a). Annual precipitation variability inferred from tree-ring width chronologies in the Changling-Shoulu region, China, during AD 1853-2007. *Dendrochronologia*, 31, 290–296.

Liu, Y., Lei, Y., Sun, B., Song, H. M. & Sun, J. Y. (2013b). Annual precipitation in Liancheng, China, since 1777 AD derived from tree rings of Chinese pine (*Pinus tabulaeformis* Carr.). *International Journal of Biometeorology*, 57, 927–934.

Liu, Y., Sun, B., Song, H. M., Lei, Y. & Wang, C. Y. (2013c). Tree-ring-based precipitation reconstruction for Mt. Xinglong, China, since AD 1679. *Quaternary International*, 283, 46–54.

Liu, Z. Y., Wen, X. Y., Brady, E. C., Otto-Bliesner, B., Yu, G., Lu, H.Y. ,et al. (2014). Chinese cave records and the East Asia summer monsoon. *Quaternary Science Reviews*, 83, 115–128.

Lu, R. Y., Dong, B. W. & Ding, H. (2006). Impact of the Atlantic multidecadal oscillation on the Asian summer monsoon. *Geophysical Research Letters*, 33, L24701.

Ma, Y. Y., Liu, Y., Song, H. M., Sun, J. Y., Lei, Y. & Wang, Y. C. (2015). A standardized precipitation evapotranspiration index reconstruction in the Taihe Mountains using tree-ring widths for the last 283 years. *Plos One*, 10, e0133605.

Menon, S., Hansen, J., Nazarenko, L. & Luo, Y. F. (2002). Climate effects of black carbon aerosols in China and India. *Science* 297, 2250–2253.

Piao, S. L., Ciais, P., Huang, Y., Shen, Z. H., Peng, S. S., Li, J. S., et al. (2010). The impacts of climate change on water resources and agriculture in China. *Nature*, 467, 43–51.

Qian, W. H., Zhu, Y. F. & Tang, S. Q. (2011). Reconstructed index of summer monsoon dry-wet modes in East Asia for the last millennium. *Chinese Science Bulletin*, 56, 3019–3027.

Rotstayn, L. D., Cai, W. J, Dix, M. R., Farquhar, G. D., Feng, Y., Ginoux, P., et al. (2007). Have Australian rainfall and cloudiness increased due to the remote effects of Asian anthropogenic aerosols? *Journal of Geophysical Research Atmospheres*, 112, D09202.

Shi, F., Fang, K. Y., Xu, C. X., Guo, Z. T., & Borgaonkar, H. P. (2017). Interannual to centennial variability of the South Asian summer monsoon over the past millennium. *Climate Dynamics*, 49, 2803–2814.

Shi, F., Li, J. P., & Wilson, R. J. S. (2014). A tree-ring reconstruction of the South Asian summer monsoon index over the past millennium. *Scientific Reports*, 4, 6739.

Song, F. F., Zhou, T. J., & Qian, Y. (2014). Responses of East Asian summer monsoon to natural and anthropogenic forcings in the latest 17 CMIP5 models. *Geophysical Research Letters*, 41, 596–603.

Song, H. M. & Liu, Y. (2011). PDSI variations at Kongtong Mountain, China, inferred from a 283-year *Pinus tabulaeformis* ring width chronology. *Journal of Geophysical Research Atmospheres*, 116, D22111.

Song, H. M., Liu, Y., Mei, R. C., Zhao, B. Y., Payompat, T. & Zhang, X. J. (2017). The

climatic response of Pinus tabulaeformis Carr. in Mt. Zhuni, Gansu. *Journal of Earth Environment*, 8(2), 119–126.

Sun, C. F., Liu, Y., Song, H. M., Mei, R. C., Payompat, T., Wang, L. & Liu, R. S. (2018). Tree-ring-based precipitation reconstruction in the source region of Weihe River, northwest China since AD 1810. *International Journal of Climatology*, 38, 3421–3431.

Tian, H. D., Stige, L. C., Cazelles, B., Kausrud, K. L., Svarverud, R., Stenseth, N. C. & Zhang, Z. B. (2011). Reconstruction of a 1,910-y-long locust series reveals consistent associations with climate fluctuations in China. *Proceedings of the National Academy of Sciences of the United States of America*, 108, 14521–14526.

Ueda, H., Kamae, Y., Hayasaki, M., Kitoh, A., Watanabe, S., Miki, Y. & Kumai, A. (2015). Combined effects of recent Pacific cooling and Indian Ocean warming on the Asian monsoon. *Nature Communications*, 6, 8854.

Waliser, D. E., Jin, K., Kang, I.-S., Stern, W. F., Schubert, S. D., Wu, M. L. C., et al. (2003). AGCM simulations of intraseasonal variability associated with the Asian summer monsoon. *Climate Dynamics*, 21, 423–446.

Wang, B. & Fan, Z. (1999). Choice of south Asian summer monsoon indices. *Bulletin of the American Meteorological Society*, 80, 629–638.

Wang, B. (2006). The Asian Monsoon. Praxis Publishing Ltd, Chichester, UK, 1–787, p183.

Wang, B., Wu, R. & Lau, K. M. (2001). Interannual Variability of the Asian Summer Monsoon: Contrasts between the Indian and the Western North Pacific–East Asian Monsoons. *Journal of Climate*, 14(20), 4073–4090.

Wang, B., Wu, Z. W., Li, J. P., Liu, J., Chang, C. P., Ding, Y. H., et al. (2008). How to

Measure the Strength of the East Asian Summer Monsoon. *Journal of Climate*, 21(17), 4449–4463.

Wang, H. J. (2001). The weakening of Asian monsoon circulation after the end of 1970's. *Advances in Atmospheric Sciences*, 18, 376–386.

Watanabe, T. & Yamazaki, K. (2014). Decadal-Scale Variation of South Asian Summer Monsoon Onset and Its Relationship with the Pacific Decadal Oscillation. *Journal of Climate*, 27, 5163–5173.

Wigley, T. M. L., Briffa, K. R. & Jones, P. D. (1984). On the average value of correlated time series, with application in dendroclimatology and hydrometeorology. *Journal of Applied Meteorology and Climatology*, 23, 201–213.

Wu, R. G. & Kirtman, B. P. (2004). The tropospheric biennial oscillation of the monsoon-ENSO system in an interactive ensemble coupled GCM. *Journal of Climate*, 17, 1623–1640.

Wu, G. X., Li, Z. Q., Fu, C. B., Zhang, X. Y., Zhang, R. Y., Zhang, R. H., et al. (2016). Advances in studying interactions between aerosols and monsoon in China. *Science China-Earth Sciences*, 59, 1-16.

Xu, H., Hong, Y. T. & Hong, B. (2012). Decreasing Asian summer monsoon intensity after 1860 AD in the global warming epoch. *Climate Dynamics*, 39, 2079–2088.

Xu, H., Lan, J. H., Sheng, E. G., Liu, B., Yu, K. K., Ye Y. D., et al. (2016). Hydroclimatic contrasts over Asian monsoon areas and linkages to tropical Pacifc SSTs. *Scientific Reports*, 6, 33177.

Xu, M., Chang, C.-P., Fu, C. B., Qi, Y., Robock, A., Robinson, D. & Zhang, H. M. (2006).

Steady decline of east Asian monsoon winds, 1969-2000: Evidence from direct ground measurements of wind speed. *Journal of Geophysical Research Atmospheres*, 111, D24111.

Yuan, L. (1994). The records of disasters in northwest China. Lanzhou: Gansu People Publishing House.

Zhang, D. E., Li, X. Q. & Liang, Y. Y. (2003). Supplement for "Yearly charts of dryness/wetness in China for the last 500–year period". *Journal of Applied Meteorological Science*, 14, 379–388.

Zhang, P. Z., Cheng, H., Edwards, R. L., Chen, F. H., Wang, Y. J., Yang, X. L., et al. (2008). A test of climate, sun, and culture relationships from an 1810-year Chinese cave record. *Science* 322, 940–942.

Zhu, C. W., Wang, B., Qian, W. H. & Zhang, B. (2012). Recent weakening of northern East Asian summer monsoon: A possible response to global warming. *Geophysical Research Letters*, 39, L09701.

Zhu, J. L., Liao, H. & Li, J. P. (2012). Increases in aerosol concentrations over eastern China due to the decadal- scale weakening of the East Asian summer monsoon. *Geophysical Research Letters*, 39, L09809.

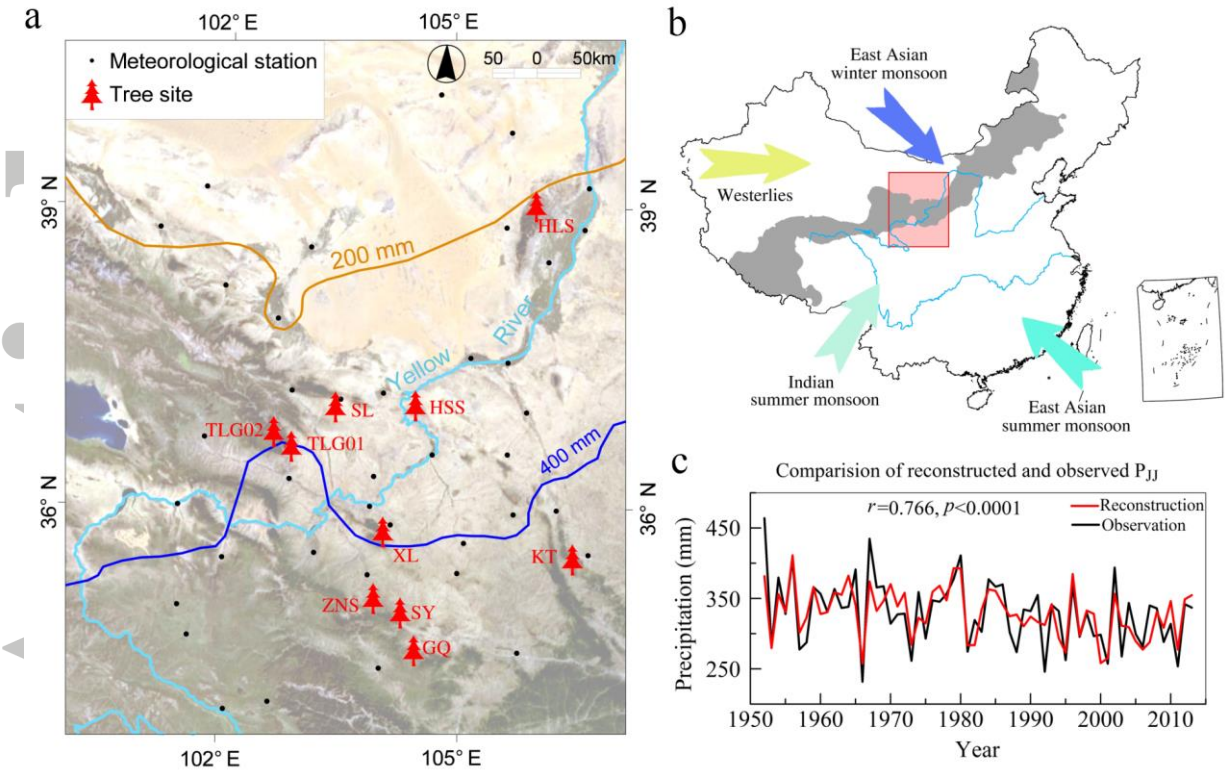

Figure 1. Location of the Asian Summer Monsoon (ASM) rainfall observations P_{JJ} (Precipitation from July of previous year to June of current year) and tree-ring samples. (a) Location of 10 tree-ring sampling sites (red tree-shapes) and 39 meteorological stations (all within the box plotted) at the northern margin of the ASM (black dots). The yellow line is the precipitation isohyet of 200 mm, and the blue is 400 mm. (b) The northern margin of the ASM (gray belt). (c) Comparison of reconstructed (red line) by tree rings and the observed (black line) precipitation data of P_{JJ} during AD 1952–2013.

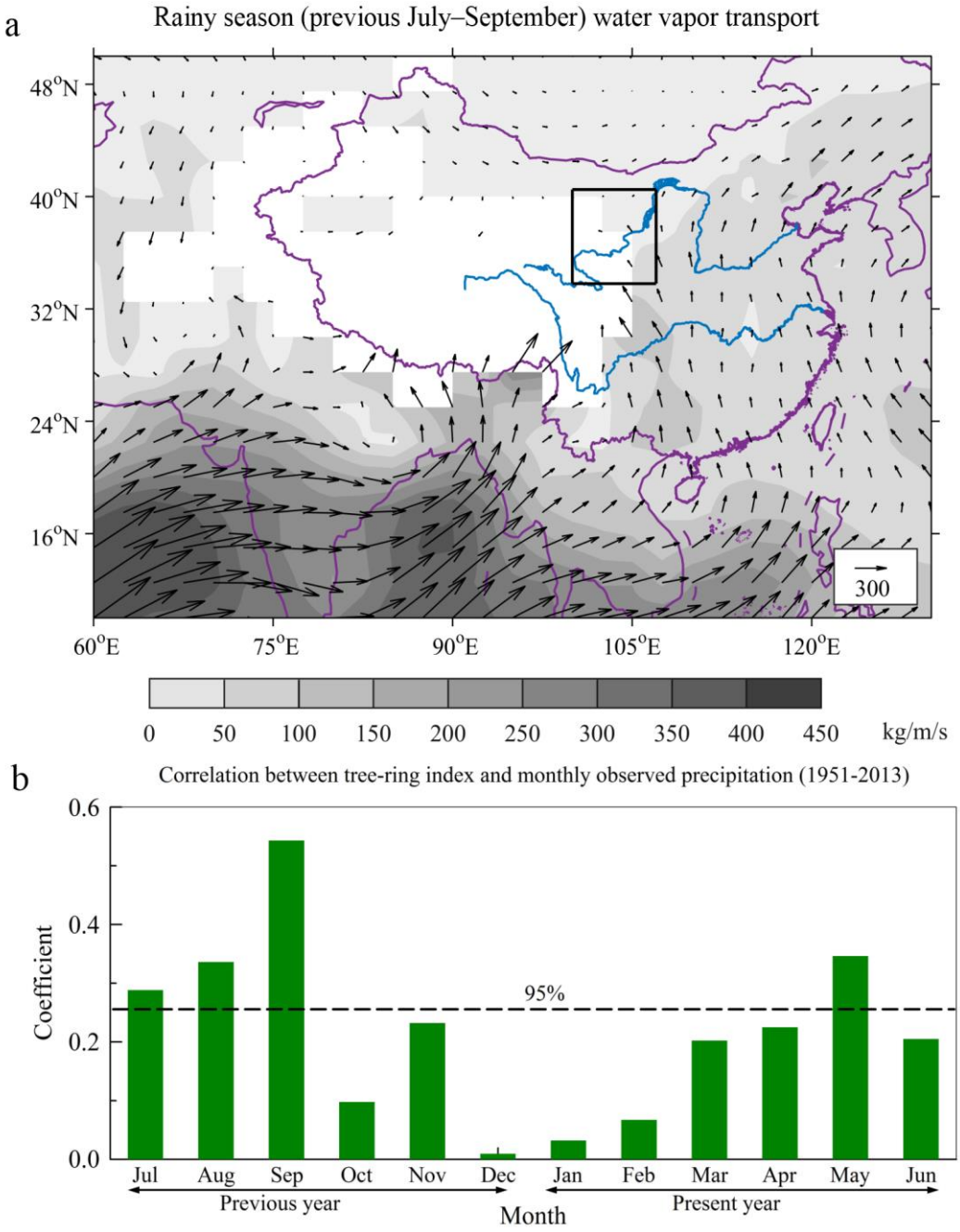

Figure 2. Representation the ASM by the reconstructed P_{JJ}. (a) Rainy season (previous July–September) water vapor transport (kg m^{-1} s^{-1}) averaged over the time span from 1952–2013 at 700 hPa of the atmospheric column and wind speed and direction based on data from NCEP/NCAR Reanalysis. Shading in (a) is the absolute value of water vapor transport of each grid. The rectangular outline represents the fringe region of the ASM (33.8°−40.5°N, 100°−107°E). (b) Correlation between ring-width chronology and observed monthly averaged mean precipitation data from 39 stations in the fringe region (1951–2013). The dashed line in (b) denotes the 95% confidence limit. The reconstructed P_{JJ} time series is a proxy for the ASM.

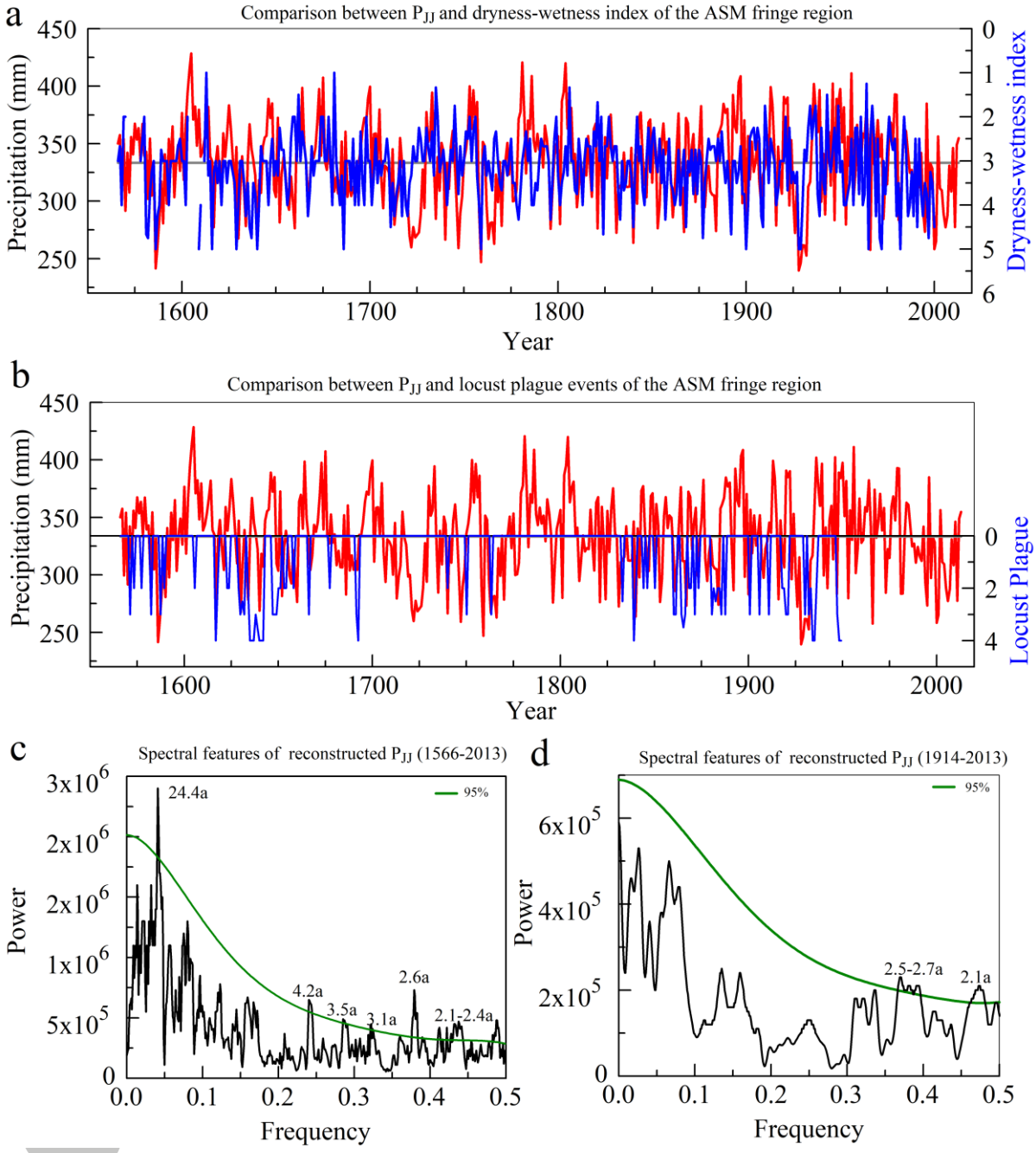

Figure 3. Properties of the reconstructed P_{JJ} index. (a) Comparison between P_{JJ} and the averaged dryness-wetness index (DWI) of the fringe region of the ASM derived from Chinese historical documents (r=-0.26, 1609–2000, p<0.001) (Chinese Academy of Meteorological Sciences, 1981; Zhang et al., 2003). The grey horizontal line denotes the mean of the ASM fringe P_{JJ} precipitation during AD 1566–2013. (b) Comparison between the P_{JJ} and the historical locust plague events in the fringe region of the ASM (Li, 2008). (c) Dominant spectral features of the reconstructed P_{JJ} during 1566–2013 obtained by using multi-taper method (MTM) spectral analyses. (d) Dominant spectral features of the reconstructed P_{JJ} during 1914–2013.

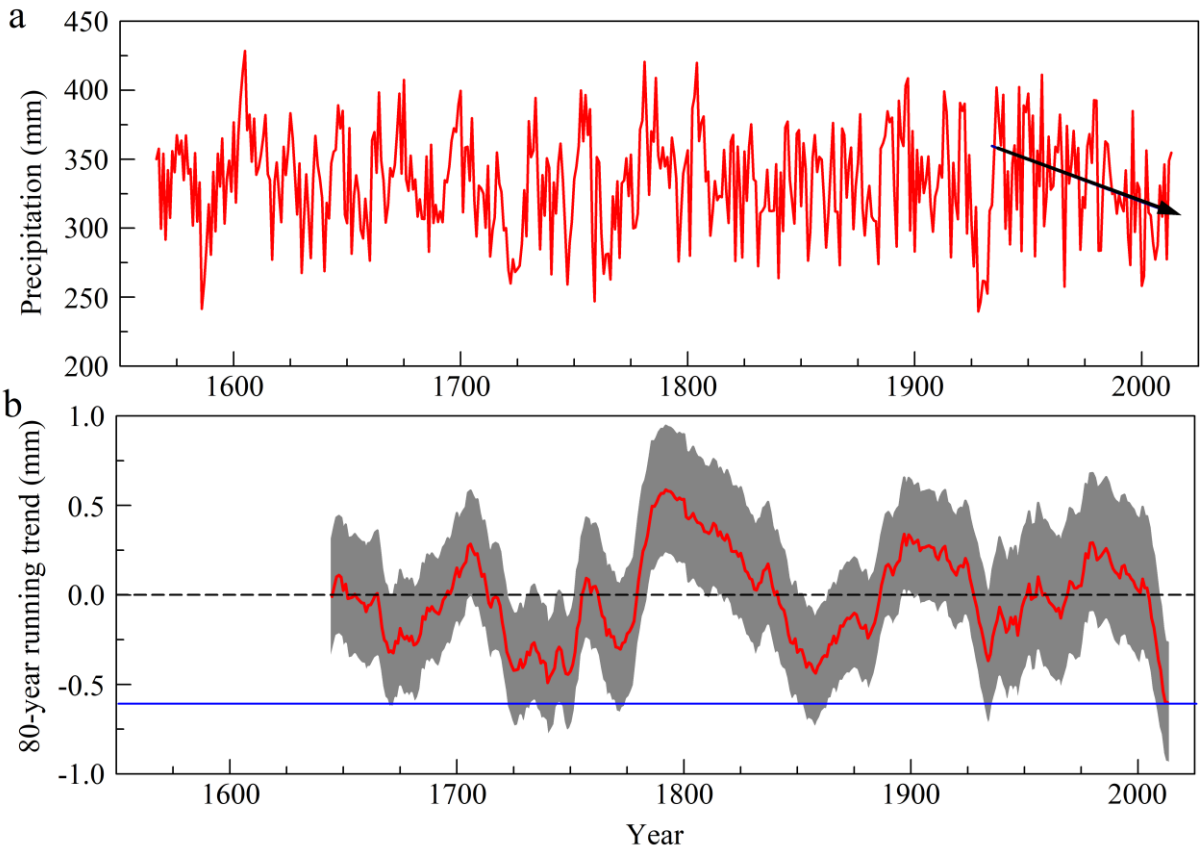

Figure 4. The reconstructed P_{JJ} time series. (a) The reconstructed P_{JJ} during the past four centuries (red curve). The sloping black line denotes an 80-year decreasing trend of P_{JJ} during the period 1934 to 2013. (b) 80-year running trend (red line) for reconstructed P_{JJ}. The gray area denotes the 95% confidence intervals. The blue horizontal line indicates the greatest 80-year decline in precipitation of ca. 0.62 mm/y.

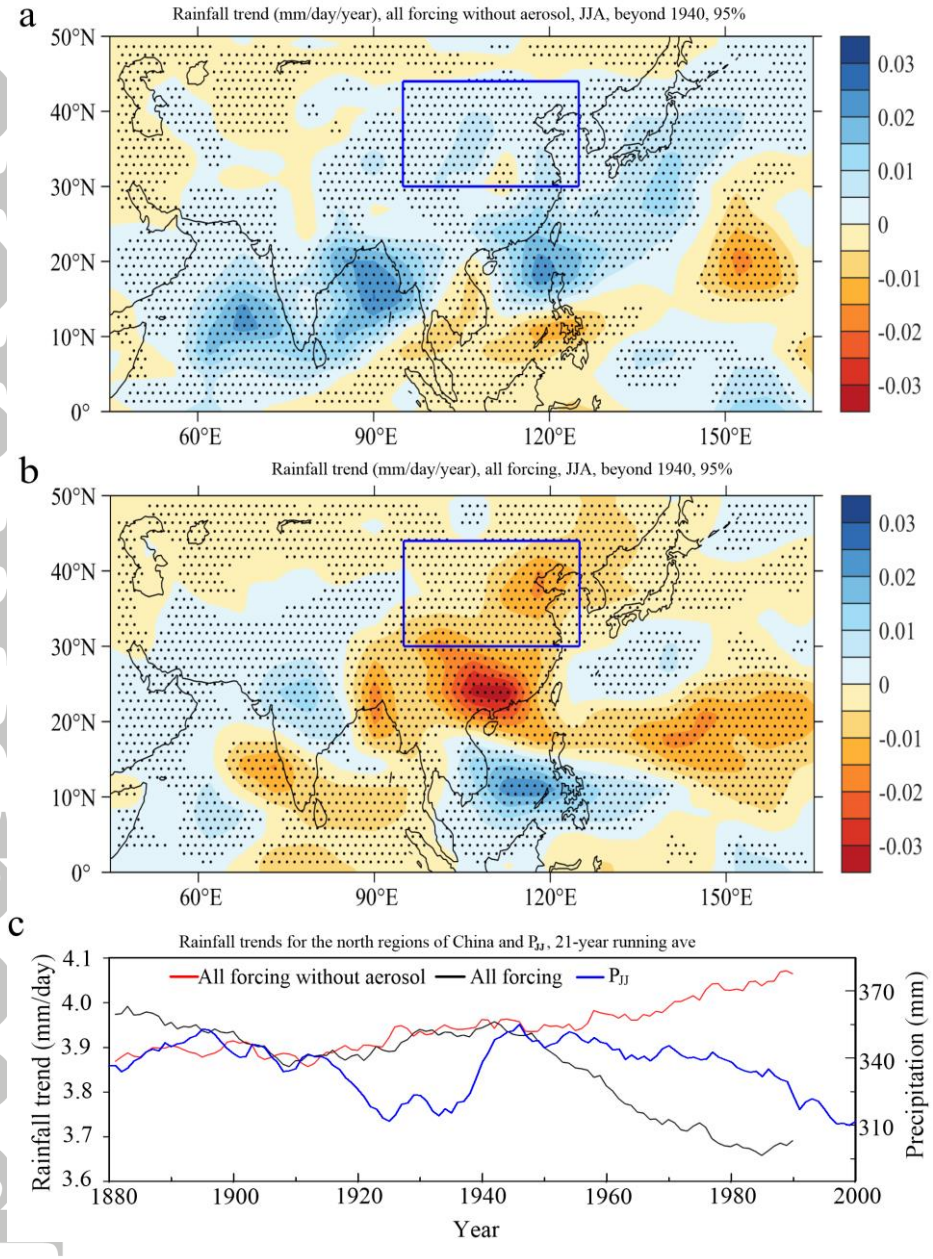

Figure 5. Boreal summer rainfall trends since 1940 simulated by a coupled climate model (Rotstayn et al., 2007). (a) All forcing but without anthropogenic aerosols. (b) All forcing including global emissions of solar irradiance, greenhouse gases, ozone, volcanic aerosols, and anthropogenic aerosols. Blue rectangular outline is the northern regions of China and the black dot indicates that the rainfall trend passes the 95% significant level. (c) Comparisons between P_{JJ} and rainfall trends for the northern regions of China. The black and red lines indicate the 21-year running averages of rainfall changes of the northern regions of China simulated from climate model and the blue line is the P_{JJ} series after applying 21-year running averages. The result shows that the decreasing trend in P_{JJ} from 1940 to 2013 is potentially contributed by anthropogenic aerosols.